

On the simultaneous scattering of two photons by a single two-level atom

Received: 10 October 2022

Accepted: 26 June 2023

Published online: 27 July 2023

 Check for updates

Luke Masters¹, Xin-Xin Hu¹, Martin Cordier¹, Gabriele Maron¹,
Lucas Pache¹, Arno Rauschenbeutel¹✉, Max Schemmer^{1,2} &
Jürgen Volz¹✉

The interaction of light with a single two-level emitter is the most fundamental process in quantum optics, and is key to many quantum applications. As a distinctive feature, two photons are never detected simultaneously in the light scattered by the emitter. This is commonly interpreted by saying that a single two-level quantum emitter can only absorb and emit single photons. However, it has been theoretically proposed that the photon anticorrelations can be thought of as arising from quantum interference between two possible two-photon scattering amplitudes, which one refers to as coherent and incoherent. This picture is in stark contrast to the aforementioned one, in that it assumes that the atom has two different mechanisms at its disposal to scatter two photons at the same time. Here we experimentally validate the interference picture by showing that, when spectrally rejecting only the coherent component of the fluorescence light of a single two-level atom, the remaining light consists of photon pairs that have been simultaneously scattered by the atom. Our results offer fundamental insights into the quantum-mechanical interaction between light and matter and open up novel approaches for the generation of highly non-classical light fields enabling, for example, Fourier-limited photon-pair sources that approach the theoretical limit in brightness.

The interaction of a single two-level quantum emitter with a near-resonant coherent light field is one of the cornerstones of quantum optics and lies at the heart of many modern experiments and applications in this field^{1–6}. The quantum-mechanical description of this interaction^{7,8} shows that the scattered light exhibits photon antibunching; that is, it never contains two photons at the same time and place^{9,10}. This property can be seen as a consequence of the photon emission being associated with quantum jumps from the emitter's excited state to its ground state. It thus seems natural to state that a single two-level atom will never scatter two photons simultaneously. However, a more in-depth inspection of the optical Bloch equations reveals the existence of two distinct components of the scattered field, referred to as coherently and incoherently scattered light, reflecting their respective ability and inability to interfere with the driving field. Taken together, these

components form the well-known Mollow structure in the fluorescence spectrum¹¹. Interestingly, when considered individually, each of these components also contains higher photon-number components, that is, two or more photons at the same time and place. In view of this fact, it has been argued that the origin of antibunching in resonance fluorescence stems from the destructive interference between the higher photon-number components of the coherently and incoherently scattered light¹². Cross-correlation measurements between the sidebands of the Mollow structure have revealed a time ordering between the detected photons, whereby the photon originating from the sideband furthest from the emitter's resonance typically arrives first^{13–15}. This is commonly interpreted as a cascaded two-photon emission from the dressed states of the emitter^{16–18}. Recently, motivated by theoretical works^{19–21}, it has been experimentally shown that by spectrally rejecting

¹Department of Physics, Humboldt Universität zu Berlin, Berlin, Germany. ²Present address: Istituto Nazionale di Ottica del Consiglio Nazionale delle Ricerche (CNR-INO), Sesto Fiorentino, Italy. ✉e-mail: arno.rauschenbeutel@hu-berlin.de; juergen.volz@hu-berlin.de

the incoherently scattered component of the fluorescence light of a single quantum dot, one can modify the photon statistics of the scattered field in such a way that all correlations are lost, and the remaining light again recovers the spectral and temporal characteristics of the classical driving field^{22,23}. In this Article we show that when performing the opposite, that is, rejecting the coherent component via spectral filtering, the remaining incoherent component of the fluorescence light of a single two-level atom consists of pairs of photons that appear to have been simultaneously scattered by the atom. Our results validate the picture that antibunching in resonance fluorescence arises from fully destructive interference between the two-photon components of the coherently and incoherently scattered light.

In more detail, we use a weak and detuned light field to excite the atom such that the coherent and incoherent components are spectrally separated while also ensuring that the latter consists purely of photon pairs (Fig. 1). To collect only the incoherently scattered light, we make use of a novel adjustable, narrowband optical notch filter to continuously reduce the amplitude of the coherently scattered light. Subsequently, we measure the second-order correlation function, $g^{(2)}(\tau)$, of the residually transmitted light. By tuning the relative magnitude of the two scattered components, we observe an evolution from a clear photon antibunching of $g^{(2)}(0) = 0.43 \pm 0.05$ without filtering to a strong photon bunching of up to $g^{(2)}(0) = 7.65 \pm 1.21$ when maximally rejecting the coherently scattered light. The latter indicates that, counterintuitively, the incoherently scattered light only consists of pairs of simultaneously scattered photons.

In our experiment we prepare a single ⁸⁵Rb atom in an optical dipole trap that is loaded from a magneto optical trap (MOT). The MOT lasers, with frequency ω_L , are red-detuned with respect to the Stark-shifted atomic resonance by $\Delta/2\pi = -57.9 \pm 3.7$ MHz. In this setting, the atom scatters photons from the MOT laser beams into free space. The quantum state of this fluorescence light can be separated into a coherent state, $|\alpha\rangle$, and an incoherently scattered component, $|\phi\rangle$, whereby the latter originates from the saturable nature of the emitter. We weakly drive the atom with a saturation parameter $S = 0.025 \pm 0.004$. In this low-saturation regime, the incoherently scattered part consists solely of photon pairs^{24–27}, with a probability amplitude for finding two photons within a time delay τ given by

$$\phi^{(2)}(\tau) = -\frac{n_{\text{coh}}}{2} e^{-(\gamma-i\Delta)|\tau|} \quad (1)$$

This wavefunction is the temporal representation of an energy–time entangled state, whereby the photons jointly propagate within a time interval $-1/\gamma$ and exhibit perfect frequency correlations. The corresponding two-photon amplitude for the coherent component is given by the time-independent value

$$\alpha^{(2)} = \frac{n_{\text{coh}}}{2} \quad (2)$$

Details are provided in the Methods. Here, $n_{\text{coh}} = \gamma S/(S+1)^2$ is the photon scattering rate of the coherent component, and $\gamma/2\pi = 3.0$ MHz (ref. 28) is the amplitude decay rate of the D₂ transition of ⁸⁵Rb. The total scattered field is given by the sum of the two components $|\psi\rangle = |\alpha\rangle + |\phi\rangle$ and for its two-photon amplitude one obtains

$$\begin{aligned} \psi^{(2)}(\tau) &= \alpha^{(2)} + \phi^{(2)}(\tau) \\ &= \frac{n_{\text{coh}}}{2} (1 - e^{-(\gamma-i\Delta)|\tau|}) \end{aligned} \quad (3)$$

Importantly, at zero time delay ($\tau = 0$), the coherently and incoherently scattered components have equal amplitude but are π out of phase. This results in perfect destructive interference such that the light never contains two simultaneously scattered photons. Despite this fact, taken

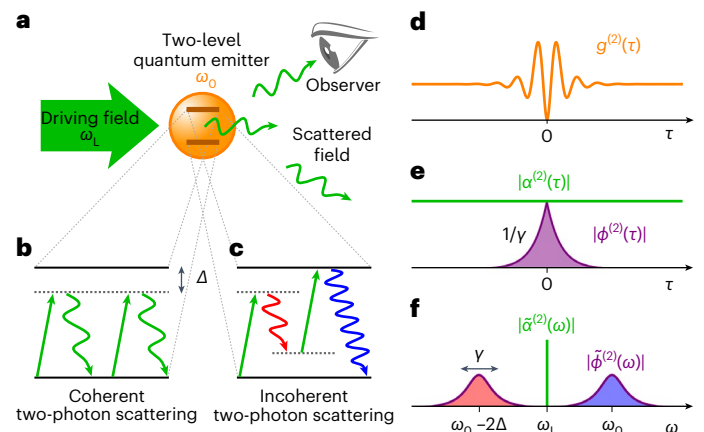


Fig. 1 | Two-photon scattering processes in resonance fluorescence.

a, Observation of resonance fluorescence from a two-level quantum emitter of resonance frequency ω_0 , driven by a light field at frequency $\omega_L = \omega_0 + \Delta$, where Δ denotes the detuning. **b**, Coherent two-photon Rayleigh scattering leads to a pair of uncorrelated photons. **c**, Incoherent two-photon scattering leads to an energy–time entangled pair of photons that are, in general, detuned from the driving field. **d**, For zero time delay τ , the theoretically predicted second-order correlation function yields $g^{(2)}(\tau=0) = 0$. For $|\tau| > 0$, Rabi oscillations are apparent. **e**, Temporal two-photon wavefunctions of the coherent and incoherent component, $\alpha^{(2)}(\tau)$ and $\phi^{(2)}(\tau)$, respectively, where $\phi^{(2)}(0) = -\alpha^{(2)}(0)$. **f**, Two-photon wavefunctions in the frequency domain. The coherent component, $\alpha^{(2)}(\omega)$, is a delta function centred at ω_L , and the incoherent component, $\phi^{(2)}(\omega)$, is given by a double Lorentzian at $\omega_L \pm \Delta$.

individually, both the coherent and incoherent components have a non-zero probability for containing two simultaneous photons.

Now, the two components exhibit different spectra, which for the coherently scattered component is given by a delta function at ω_L , whereas for the incoherently scattered component, at low saturation, the spectrum is approximately given by a pair of Lorentzian lines, each of width γ , which are separated by $\pm\Delta$ from ω_L (ref. 8; Fig. 1). Their distinct spectra allow us to separate the components by applying a frequency notch filter centred at the driving laser frequency. For this, we first collect the atomic fluorescence with a high-numerical-aperture (NA) objective before coupling it into a single-mode fibre, which guides the light to the filter (Fig. 2). The latter is realised by means of a fibre-ring resonator, where we use a low-loss variable-ratio fibre beamsplitter to control the coupling rate into the resonator, κ_{ext} , and in turn the on-resonance transmission past the resonator (Fig. 2, right inset). The resonator is stabilized to resonance with the driving laser and has an extremely narrow linewidth that is adjustable between 1 and 15 MHz, which is much smaller than the separation of the coherent and incoherent components of $|\Delta|$. As a consequence, the filter reduces the coherent component by the κ_{ext} -dependent complex-valued field transmission factor, $t_{\text{coh}}(\kappa_{\text{ext}})$, but does not substantially alter the incoherent component (Methods). To measure the modified photon statistics after filtering, we send the light to a Hanbury Brown and Twiss set-up consisting of a 50/50 beamsplitter and a single-photon counter in each of its outputs²⁹, and record the second-order correlation function, $g^{(2)}(\tau, \kappa_{\text{ext}}) \propto |t_{\text{coh}}(\kappa_{\text{ext}})|^2 \alpha^{(2)} - \phi^{(2)}(\tau)|^2$, for different settings of the coupling parameter κ_{ext} .

Figure 3 showcases the second-order correlation functions as κ_{ext} is increased. For $\kappa_{\text{ext}} = 0$, the filter resonator has no effect on the collected atomic fluorescence. The resulting measured second-order correlation function (purple) is $g^{(2)}(0) = 0.43 \pm 0.05$, which is compatible with perfect photon antibunching when considering the background count rates of our photon counters. This illustrates the expected behaviour whereby, in the absence of spectral selection, the light scattered by a single atom never contains more than one photon at the same time

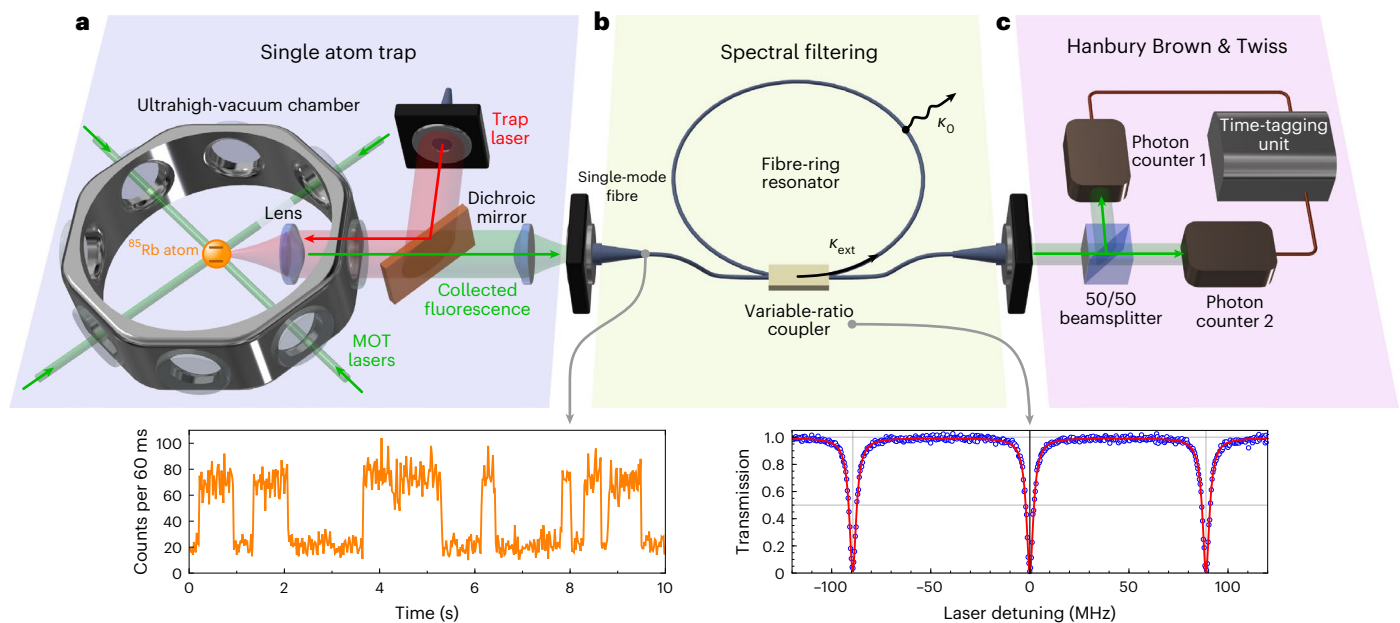


Fig. 2 | Experimental set-up. **a**, A single ^{85}Rb atom is loaded from a MOT into an optical dipole trap. Fluorescence photons from the atom are collected with a lens (NA = 0.55), separated from the trapping laser with a dichroic mirror, and coupled into a single-mode fibre. Inset: measured time trace of the photon count rate, indicating the presence or absence of a single atom inside the trap. **b**, The collected fluorescence is fibre-guided to an optical notch filter realised by means of a fibre-ring resonator. A variable-ratio coupler allows for control over the coupling rate, κ_{ext} , into the resonator, which has an intrinsic loss rate of κ_0 . A piezo-electric fibre stretcher (not displayed) is used for stabilization of the

resonator to the MOT laser frequency ω_L . A fibre-polarization controller (not displayed) is used to compensate for birefringence to realise a non-polarization-selective filter operation. Inset: transmission spectrum for the critically coupled filter resonator, that is, when $\kappa_{\text{ext}} = \kappa_0$. This spectrum shows a full-width at half-maximum linewidth of 4.4 MHz with a free spectral range of 89.1 MHz. **c**, The filtered fluorescence light is sent to a Hanbury Brown and Twiss set-up consisting of a pair of single-photon counters behind a 50/50 beamsplitter. Photon arrival times are recorded by a time-tagging unit, from which we measure the second-order correlation function, $g^{(2)}(\tau)$, of the filtered light.

and place. For $|\tau| > 0$, we observe a damped oscillatory behaviour, originating from the driven atom undergoing Rabi oscillations at an effective frequency of $\Omega_{\text{eff}} \approx \Delta$, which are dampened on the timescale of the excited-state lifetime, $1/2\gamma$. This oscillatory behaviour can also be considered to originate from interference between the coherently and incoherently scattered two-photon components, (equation (3)).

When increasing κ_{ext} , the power transmission, $|t_{\text{coh}}(\kappa_{\text{ext}})|^2$, of the coherent component through the filter is reduced. Consequently, we upset the delicate balance of the two components, resulting in less destructive interference and hence increasing $g^{(2)}(\tau=0)$ (blue and green datasets). Around $\kappa_{\text{ext}} \approx \kappa_0$, the coherent component is strongly attenuated. Consequently, the second-order correlation function resembles a double-exponential envelope centred at $\tau = 0$, featuring strong photon bunching of up to $g^{(2)}(\tau=0) = 7.65 \pm 1.21$ (yellow and orange datasets). When further increasing κ_{ext} , the transmission, $t_{\text{coh}}(\kappa_{\text{ext}})$, of the coherent component will increase again, and the bunching decreases (red and violet datasets). For very large values of κ_{ext} , antibunching would be recovered, although it is not observed here for technical reasons.

Figure 4 shows the evolution of the measured second-order correlation function at $\tau = 0$, as a function of κ_{ext} . For each setting, the value of $g^{(2)}(0, \kappa_{\text{ext}})$ is obtained by averaging the data shown in Fig. 3 in a 3-ns window centred around $\tau = 0$. The solid orange curve is the theoretical prediction of $g^{(2)}(0, \kappa_{\text{ext}})$ (Methods). We note that our model takes into account residual drifts of the filter resonance, which we obtain from fits to the datasets in Fig. 3 (Methods). As a consequence of these drifts, maximum suppression of the coherently scattered component is reached for a setting of κ_{ext} slightly larger than κ_0 . Across all settings of our filter, we observe a beating in the second-order correlation function resulting from the interference between the incoherently and remaining coherently scattered two-photon components, once again illustrating their coherence with respect to each other. For perfect

suppression of the coherent component, these oscillations vanish and the $g^{(2)}(\tau)$ would exhibit a pure double-exponential decay centred at $\tau = 0$, with a decay time of $1/2\gamma$.

From the two datasets exhibiting the best suppression of the coherently scattered light ($\kappa_{\text{ext}} = 1.00\kappa_0$ and $\kappa_{\text{ext}} = 2.23\kappa_0$), we obtain a rate of detected photon pairs of $n_{\text{meas.}}^{(2)} = (4.91 \pm 0.47) \times 10^{-3} \text{ s}^{-1}$ (Methods). Given the pair detection efficiency $\eta^2/2$ of our set-up, this corresponds to a total rate of photon pairs incoherently scattered by the atom of $n_{\text{total}}^{(2)} = 5.3 \pm 0.5 \text{ kHz}$. This agrees well with the rate of incoherently scattered photon pairs, $n_{\text{inc}}/2 = 5.7 \pm 1.4 \text{ kHz}$, that is expected for our saturation parameter (Methods). Note, that n_{inc} is much smaller than the rate of coherently scattered photons, $n_{\text{coh}} = 455 \pm 55 \text{ kHz}$, and, as the ratio of these two components is given by S , for a vanishing saturation, the relative contribution of the incoherent component tends to zero. Yet, intriguingly, when interfering with the coherent component, its small but finite value is still necessary for the observation of photon antibunching.

To conclude, we return to the initial discussion on whether a single two-level atom will simultaneously scatter two photons. As is often the case in quantum mechanics, the answer is both yes and no, depending on which picture is considered. Indeed, the unmodified light field emitted by the atom never contains two simultaneous photons. Here, we have highlighted the picture where this is a consequence of the atom continuously scattering the incident two-photon component in two different ways—coherently and incoherently—which perfectly destructively interfere to yield antibunched photon statistics. An alternative picture is to state that the atom only scatters photons one by one, and that the emitted stream of antibunched photons is transformed into bunched photons by the passive linear notch filter in our set-up. In this picture, the resonator acts as a storage medium for the scattered light, and Hong–Ou–Mandel quantum interference³⁰ at the

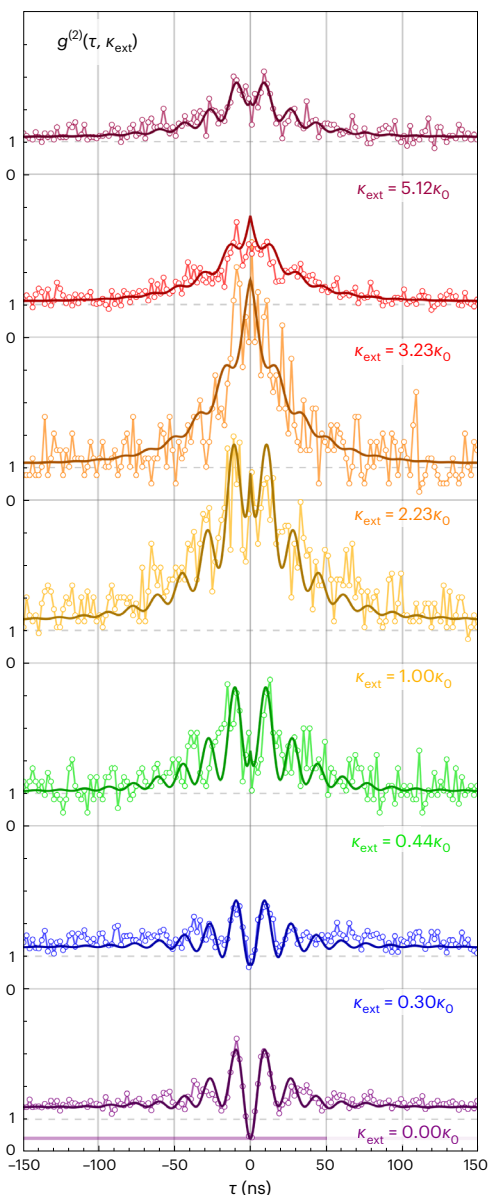


Fig. 3 | Measured second-order correlation functions $g^{(2)}(\tau)$ for different filter settings κ_{ext} . Each dataset has the same vertical scale. The solid lines are fits of our theoretical model to the data points (open circles), with the temperature of the trapped atom and a residual resonator–laser detuning as fit parameters (Methods). For the unfiltered dataset ($\kappa_{\text{ext}} = 0$), the purple horizontal line indicates the noise floor due to background counts.

incoupling beamsplitter between the incoming fluorescence light and the stored field results in photon bunching of the light transmitted past the resonator (Methods). Beyond these fundamental considerations, the demonstrated effect lends itself to realising spectrally narrowband photon-pair sources that are inherently compatible with optical transitions in quantum emitters^{31,32} (Methods). In particular, for high photon collection efficiencies^{33–35}, the achievable photon-pair rate would approach the theoretical limit in brightness of a Fourier-limited pair source. Consequently, we envision that photon-pair sources based on this effect will emerge as a key resource in optical quantum technologies and quantum information processing.

Online content

Any methods, additional references, Nature Portfolio reporting summaries, source data, extended data, supplementary information,

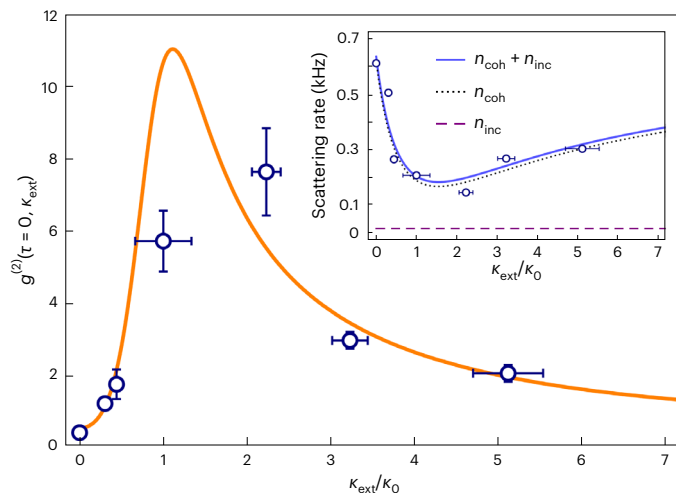


Fig. 4 | Correlations at zero time delay as a function of filter setting. The data points show the measured value of $g^{(2)}(\tau = 0, \kappa_{\text{ext}})$ averaged over a 3-ns window centred around $\tau = 0$. The horizontal error bars indicate the 1σ uncertainty in the setting of κ_{ext} , and the vertical error bars indicate the statistical 1σ uncertainty interval obtained from the number of detected photon pairs for each setting. The solid line is the theoretical prediction (details are provided in the main text). Inset: dark count corrected detected photon rate after filtering (data points), with the corresponding theory prediction (blue solid line), which contains the single-photon detection efficiency η as the only fit parameter. From the fit we obtain $\eta = 0.136 \pm 0.002\%$. The individual contributions to the scattering rate are depicted by the black dotted (coherent) and purple dashed (incoherent) lines. The horizontal error bars are the same as in the main figure, and those in the vertical direction are not visible on the scale of the inset.

acknowledgements, peer review information; details of author contributions and competing interests; and statements of data and code availability are available at <https://doi.org/10.1038/s41566-023-01260-7>.

References

1. Walmsley, I. A. Quantum optics: science and technology in a new light. *Science* **348**, 525–530 (2015).
2. Gisin, N. & Thew, R. Quantum communication. *Nat. Phot.* **1**, 165–171 (2007).
3. Ladd, T. D. et al. Quantum computers. *Nature* **464**, 45–53 (2010).
4. Kimble, H. J. The Quantum Internet. *Nature* **453**, 1023–1030 (2008).
5. Eisaman, M. D., Fan, J., Migdall, A. & Polyakov, S. V. Invited review article: single-photon sources and detectors. *Rev. Sci. Instrum.* **82**, 071101 (2011).
6. Aharonovich, I., Englund, D. & Toth, M. Solid-state single-photon emitters. *Nat. Phot.* **10**, 631–641 (2016).
7. Gerry, C. & Knight, P. *Introductory Quantum Optics* (Cambridge Univ. Press, 2004).
8. Steck, D. A. *Quantum and Atom Optics* (Open Publication License, 2007); <https://atomoptics.uoregon.edu/~dsteck/teaching/quantum-optics/>
9. Carmichael, H. J. & Walls, D. F. Proposal for the measurement of the resonant Stark effect by photon correlation techniques. *J. Phys. B At. Mol. Phys.* **9**, L43 (1976).
10. Kimble, H. J., Dagenais, M. & Mandel, L. Photon antibunching in resonance fluorescence. *Phys. Rev. Lett.* **39**, 691–695 (1977).
11. Mollow, B. R. Power spectrum of light scattered by two-level systems. *Phys. Rev.* **188**, 1969–1975 (1969).
12. Dalibard, J. & Reynaud, S. Correlation signals in resonance fluorescence: interpretation via photon scattering amplitudes. *J. Phys.* **44**, 1337–1343 (1983).

13. Aspect, A., Roger, G., Reynaud, S., Dalibard, J. & Cohen-Tannoudji, C. Time correlations between the two sidebands of the resonance fluorescence triplet. *Phys. Rev. Lett.* **45**, 617–620 (1980).
14. Ulhaq, A. et al. Cascaded single-photon emission from the mollow triplet sidebands of a quantum dot. *Nat. Phot.* **6**, 238–242 (2012).
15. Ng, B. L., Chow, C. H. & Kurtsiefer, C. Observation of the Mollow triplet from an optically confined single atom. *Phys. Rev. A* **106**, 063719 (2022).
16. Cohen-Tannoudji, C. & Reynaud, S. Dressed-atom description of resonance fluorescence and absorption spectra of a multi-level atom in an intense laser beam. *J. Phys. B. At. Mol. Phys.* **10**, 345 (1977).
17. Arnoldus, H. F. & Nienhuis, G. Photon correlations between the lines in the spectrum of resonance fluorescence. *J. Phys. B. At. Mol. Phys.* **17**, 963–977 (1984).
18. Schrama, C. A., Nienhuis, G., Dijkerman, H. A., Steijlsiger, C. & Heideman, H. G. M. Intensity correlations between the components of the resonance fluorescence triplet. *Phys. Rev. A* **45**, 8045–8055 (1992).
19. del Valle, E., Gonzalez-Tudela, A., Laussy, F. P., Tejedor, C. & Hartmann, M. J. Theory of frequency-filtered and time-resolved n-photon correlations. *Phys. Rev. Lett.* **109**, 183601 (2012).
20. Carreño, J. C. L., Casalengua, E. Z., Laussy, F. P. & del Valle, E. Joint subnatural-linewidth and single-photon emission from resonance fluorescence. *Quantum Sci. Technol.* **3**, 045001 (2018).
21. Casalengua, E. Z., Carreño, J. C. L., Laussy, F. P. & del Valle, E. Conventional and unconventional photon statistics. *Laser Photon. Rev.* **14**, 1900279 (2020).
22. Hanschke, L. et al. Origin of antibunching in resonance fluorescence. *Phys. Rev. Lett.* **125**, 170402 (2020).
23. Phillips, C. L. et al. Photon statistics of filtered resonance fluorescence. *Phys. Rev. Lett.* **125**, 043603 (2020).
24. Shen, J.-T. & Fan, S. Strongly correlated multiparticle transport in one dimension through a quantum impurity. *Phys. Rev. A* **76**, 062709 (2007).
25. Mahmoodian, S. et al. Strongly correlated photon transport in waveguide quantum electrodynamics with weakly coupled emitters. *Phys. Rev. Lett.* **121**, 143601 (2018).
26. Prasad, A. S. et al. Correlating photons using the collective nonlinear response of atoms weakly coupled to an optical mode. *Nat. Phot.* **14**, 719–722 (2020).
27. Hinney, J. et al. Unraveling two-photon entanglement via the squeezing spectrum of light traveling through nanofiber-coupled atoms. *Phys. Rev. Lett.* **127**, 123602 (2021).
28. Steck, D. A. Rubidium 85 D line data. Revision 2.2.3 (9 July 2021); <http://steck.us/alkalidata>
29. Brown, R. H. & Twiss, R. Q. Correlation between photons in two coherent beams of light. *Nature* **177**, 27–29 (1956).
30. Hong, C. K., Ou, Z. Y. & Mandel, L. Measurement of subpicosecond time intervals between two photons by interference. *Phys. Rev. Lett.* **59**, 2044–2046 (1987).
31. Carreño, J. C. L., Feijoo, S. B. & Stobińska, M. Entanglement in resonance fluorescence. Preprint at <https://doi.org/10.48550/arXiv.2302.04059> (2023).
32. Casalengua, E. Z., del Valle, E. & Laussy, F. P. Two-photon correlations in detuned resonance fluorescence. *Phys. Script.* **98**, 055104 (2023).
33. Fischer, M. et al. Efficient saturation of an ion in free space. *Appl. Phys. B* **117**, 797–801 (2014).
34. Arcari, M. et al. Near-unity coupling efficiency of a quantum emitter to a photonic crystal waveguide. *Phys. Rev. Lett.* **113**, 093603 (2014).
35. Abudayyeh, H. et al. Single photon sources with near unity collection efficiencies by deterministic placement of quantum dots in nanoantennas. *APL Photonics* **6**, 036109 (2021).

Publisher's note Springer Nature remains neutral with regard to jurisdictional claims in published maps and institutional affiliations.

Open Access This article is licensed under a Creative Commons Attribution 4.0 International License, which permits use, sharing, adaptation, distribution and reproduction in any medium or format, as long as you give appropriate credit to the original author(s) and the source, provide a link to the Creative Commons license, and indicate if changes were made. The images or other third party material in this article are included in the article's Creative Commons license, unless indicated otherwise in a credit line to the material. If material is not included in the article's Creative Commons license and your intended use is not permitted by statutory regulation or exceeds the permitted use, you will need to obtain permission directly from the copyright holder. To view a copy of this license, visit <http://creativecommons.org/licenses/by/4.0/>.

© The Author(s) 2023

Methods

Theoretical description

Wavefunction description of the scattered field. In a standard picture, the atom–light interaction is described by optical Bloch equations, in which the atom is excited by a coherent laser beam and the scattered quantum field can be calculated from the time evolution of the atomic raising and lowering operators⁸. In the steady state, the scattered field exhibits two distinct components, usually referred to as coherently and incoherently scattered light, and their ratio depends on the saturation parameter of the excitation laser field

$$S = \frac{1}{2} \frac{(\Omega/\gamma)^2}{1 + (\Delta/\gamma)^2} \quad (4)$$

Here, $\Delta = \omega_L - \omega_0$ is the laser–atom detuning with laser frequency ω_L and atomic resonance frequency ω_0 . Ω is the Rabi frequency of the driving field and γ is the amplitude decay rate of the excited state. The coherent and incoherent scattering rates of the atom are given by

$$n_{\text{coh}} = \gamma \frac{S}{(S+1)^2} \approx \gamma(S - 2S^2) \quad (5)$$

and

$$n_{\text{inc}} = \gamma \frac{S^2}{(S+1)^2} \approx \gamma S^2 \quad (6)$$

respectively, where the right-hand-side expressions are the low saturation expansions up to second order in S , which we apply throughout the manuscript to obtain a simple theoretical description of the scattered light. In the following, we consider the case where we drive the atom with an excitation laser beam for time duration T , where T is chosen such that it is much larger than the atomic decay time, $T \gg 1/\gamma$ (to neglect transient features), and small enough that the mean photon number is much smaller than one, that is, $T \ll 1/\gamma S$. We note that in the low saturation regime, $S \ll 1$, this is always possible. The coherently scattered light can then be represented as a coherent state

$$|\alpha\rangle \approx |0\rangle + \alpha |1\rangle + \frac{\alpha^2}{\sqrt{2}} |2\rangle \quad (7)$$

with mean photon number $\alpha^2 = n_{\text{coh}} T$, where, without loss of generality, we assume α to be real. In the time domain, in a frame rotating with the laser frequency, the two-photon component of the state can be written as

$$\frac{\alpha^2}{\sqrt{2}} |2\rangle = \iint_{-T/2}^{T/2} dt_1 dt_2 \frac{\alpha^2}{2T} a_{t_1}^\dagger a_{t_2}^\dagger |0\rangle \quad (8)$$

where a_t^\dagger (a_t) is the creation (annihilation) operator for a photon at time t , and $\alpha^{(2)} = n_{\text{coh}}/2$ is the amplitude of the two-photon wavefunction. In the low saturation limit, the incoherently scattered light consists of energy–time entangled photon pairs^{24–27} and the state in the time domain can be written as

$$|\phi\rangle = \iint_{-T/2}^{T/2} dt_1 dt_2 \phi^{(2)}(t_2 - t_1) a_{t_1}^\dagger a_{t_2}^\dagger |0\rangle \quad (9)$$

Here, the integrals extend over time duration T and the temporal envelope $\phi^{(2)}(\tau)$ is given by

$$\phi^{(2)}(\tau) = -\frac{n_{\text{coh}}}{2} e^{-(\gamma-i\Delta)|\tau|} \quad (10)$$

The total scattered field is thus given by

$$|\psi\rangle = |\alpha\rangle + |\phi\rangle \quad (11)$$

and for its two-photon component one obtains

$$|\psi^{(2)}\rangle = \frac{n_{\text{coh}}}{2} \iint_{-T/2}^{T/2} dt_1 dt_2 [1 - e^{-(\gamma-i\Delta)(t_2-t_1)}] a_{t_1}^\dagger a_{t_2}^\dagger |0\rangle \quad (12)$$

Modelling the photon statistics. The spectral distributions of the two components differ from each other; the spectrum of the coherent state $|\alpha\rangle$ is approximately given by a delta function at laser frequency ω_L , whereas the spectrum of the incoherently scattered component, at low saturation, is approximately given by a pair of Lorentzian lines centred at frequencies $\omega_L \pm \Delta$. This frequency separation between the coherent and incoherent components allows us to separate them by using a narrowband notch filter at the laser frequency, which in our experiment is realised as a fibre-ring resonator. The complex-valued field transmission factor³⁶ of the resonator is given by

$$t_F(\omega, \kappa_{\text{ext}}) = \frac{\kappa_0 - \kappa_{\text{ext}} + i(\omega - \omega_{\text{res}})}{\kappa_0 + \kappa_{\text{ext}} + i(\omega - \omega_{\text{res}})} \quad (13)$$

Here, κ_{ext} is the external coupling rate into the filter resonator, κ_0 is the intrinsic loss rate of the filter resonator, and ω_{res} is its resonance frequency. As the filter bandwidth is much smaller than the separation of the frequency components, in the following we make the simplifying assumption that the filter acts only on the coherently scattered light and reduces its field amplitude by the κ_{ext} -dependent transmission factor $t_{\text{coh}}(\kappa_{\text{ext}}) \equiv t_F(\omega_L, \kappa_{\text{ext}})$, as presented in the main text. The wavefunction of the light after filtering is then given by

$$|\psi_F\rangle = |t_{\text{coh}}(\kappa_{\text{ext}})\alpha\rangle + |\phi\rangle \quad (14)$$

and the corresponding envelope of the two-photon wavefunction is given by

$$\psi_F^{(2)}(\tau) = \frac{n_{\text{coh}}}{2} [t_{\text{coh}}(\kappa_{\text{ext}})^2 - e^{-(\gamma-i\Delta)|\tau|}] \quad (15)$$

In our experiment, we analyse the photon statistics of the filtered atomic fluorescence by measuring its second-order correlation function

$$G^{(2)}(\tau) = \frac{\langle a_t^\dagger a_{t+\tau}^\dagger a_{t+\tau} a_t \rangle_t}{\langle a_t^\dagger a_t \rangle_t^2} \equiv \frac{G^{(2)}(\tau)}{n^2} \quad (16)$$

where $\langle \dots \rangle_t$ indicates the time-averaged expectation value and $\tau = t_2 - t_1$ is the temporal separation between the two photons. $G^{(2)}(\tau) \propto \eta^2 |\psi_F^{(2)}|^2$ is the unnormalized second-order correlation function, for which we obtain from equation (15)

$$G^{(2)}(\tau) \approx \gamma^2 S^2 \eta^2 |t_{\text{coh}}(\kappa_{\text{ext}})^2 - e^{-(\gamma-i\Delta)|\tau|}|^2 \quad (17)$$

The mean photon flux, n , after the filter is given by

$$n = \gamma S \eta (|t_{\text{coh}}(\kappa_{\text{ext}})|^2 (1 - 2S) + S) = \eta (|t_{\text{coh}}(\kappa_{\text{ext}})|^2 n_{\text{coh}} + n_{\text{inc}}) \quad (18)$$

Here we introduce the total single-photon collection and detection efficiency of our set-up, η . In the experiment, in addition to the measured photon rate, we also have to take into account the total

background count rate, d , that originates from stray light and detector dark counts. Including this background in the experimentally expected second-order correlation function, we obtain

$$g_{\text{exp}}^{(2)}(\tau) \approx \frac{G^{(2)}(\tau) - n^2}{(n + d)^2} + 1 \quad (19)$$

Description in the time domain. It has been shown that the spectral filtering of coherent light can alter its statistical properties, such that the phase noise of, for example, a laser light field³⁷, is changed into intensity fluctuations by a narrow linear filter, resulting in chaotic light in its output. Although such a classical reasoning cannot be applied to our experiment, the transformation of the stream of antibunched photons emitted by the atom into a stream of bunched photons after the notch filter can still be explained by evoking Hong–Ou–Mandel quantum interference³⁰. To this end, we make use of the fact that the resonator has a slow temporal response to the light field with a characteristic timescale of $(\kappa_0 + \kappa_{\text{ext}})^{-1}$ that is much slower than the amplitude fluctuations in the atomic fluorescence, which are on a timescale of Δ^{-1} . Consequently, the resonator averages over these fluctuations and, in the steady state, the light stored in the resonator can approximately be described by a coherent state with amplitude

$$\alpha_r = -\sqrt{n_{\text{coh}}} \frac{\sqrt{2\kappa_{\text{ext}}}}{i(\omega - \omega_{\text{res}}) + \kappa_{\text{ext}} + \kappa_0} \quad (20)$$

To calculate the probability of a photon coincidence detection with time delay τ after the filter resonator, we have to consider the different ways in which such a detection event can occur. In this picture, there are two fields, the resonator field and the incident fluorescence, which are overlapped on the incoupling beamsplitter of the resonator. Two photons can either both originate from the original fluorescence light (amplitude, $\psi_f^{(2)}$), both from the resonator (amplitude, $\psi_r^{(2)}$) or one photon from each (amplitude, $\psi_{fr}^{(2)}$). Note that the incoupling beamsplitter is highly asymmetric with a transmission of approximately one for the incident fluorescence light. The three probability amplitudes are then given by

$$\psi_f^{(2)} = \frac{n_{\text{coh}}}{2} (1 - e^{-(\gamma-i\Delta)|\tau|}) \quad (21)$$

$$\psi_r^{(2)} = \frac{(-\alpha_r \sqrt{2\kappa_{\text{ext}}})^2}{2} = \frac{n_{\text{coh}}}{2} (t_{\text{coh}}(\kappa_{\text{ext}}) - 1)^2 \quad (22)$$

$$\psi_{fr}^{(2)} = -\sqrt{n_{\text{coh}}} \sqrt{2\kappa_{\text{ext}}} \alpha_r = n_{\text{coh}} (t_{\text{coh}}(\kappa_{\text{ext}}) - 1) \quad (23)$$

The total two-photon detection probability amplitude is the coherent sum of the three components, and for the two-photon field after the resonator we obtain

$$\begin{aligned} \psi_F^{(2)} &= \psi_f^{(2)} + \psi_r^{(2)} + \psi_{fr}^{(2)} \\ &= \frac{n_{\text{coh}}}{2} \left[t_{\text{coh}}(\kappa_{\text{ext}})^2 - e^{-(\gamma-i\Delta)|\tau|} \right] \end{aligned} \quad (24)$$

This is the same expression as equation (15), which demonstrates the equivalence of the two pictures.

Implementing a photon-pair source. Using the filtering technique presented in this Article to remove the coherently scattered light lends itself to realising spectrally narrowband energy–time entangled photon-pair sources that are inherently compatible with optical transitions in quantum emitters. As it relies on the fundamental mechanism of resonance fluorescence, this technique can be utilized with any two-level emitter. The crucial figure of merit for such a photon-pair

source is the achievable photon pair rate. In general, the rate of photon pairs, n_p , after the optical filtering is given by

$$n_p \lesssim \eta^2 \frac{n_{\text{inc}}}{2} = \eta^2 \frac{\gamma}{2} \frac{S^2}{(S+1)^2} \quad (25)$$

where η is the photon collection efficiency of the optical set-up. Note that, in this inequality, $n_p \approx \eta^2 n_{\text{inc}}/2$ only holds for $S < 1$. For close-to-unity collection efficiencies that can be realised using high-NA optics³³ or solid-state quantum emitters with integrated structures^{34,35}, the maximum entangled photon pair rate that can be realised is bounded by $\gamma/2$ for large saturation powers. This is the fundamental limit that can be achieved for any source of photon pairs with linewidth γ , as otherwise the temporal separation of subsequent photon pairs is smaller than their extension in time, $\sim 1/\gamma$. Consequently, one can conclude that for high photon-collection efficiencies, the filtered resonance fluorescence yields an ideal source of photon pairs. Comparison with alternative theoretical models³⁸ shows that our theoretical description should be valid for saturation parameters of $S \lesssim 0.25$, otherwise the incoherent component also contains higher-order photon-scattering processes. For $S = 0.25$, one would obtain a pair source with photon-pair rates of $n_p = \gamma/50 \approx 4 \times 10^5$ pairs per second with a bandwidth of $\gamma = 2\pi \times 3$ MHz, which is substantially better than state-of-the-art photon-pair sources with a comparable bandwidth³⁹.

Effect of non-perfect filtering. Imperfect filtering of the coherent light, that is, $|t_{\text{coh}}| > 0$, would lead to a background of coherently scattered photons. The ratio of the coherent to incoherent components after optical filtering is given by

$$\frac{n_{\text{inc}}}{n_{\text{coh}}} = \frac{S}{|t_{\text{coh}}|^2} \quad (26)$$

For a low background of coherently scattered photons, this signal-to-noise ratio should be much larger than one. For saturation parameters around $S \approx 0.1$, this can be readily achieved with a residual filter transmission of $|t_{\text{coh}}|^2 \approx 1\%$.

Experimental methods

Trapping and detecting single atoms. We prepared a cloud of ⁸⁵Rb atoms inside an ultrahigh-vacuum chamber using a MOT. The MOT lasers, with frequency ω_L , are red-detuned with respect to the unperturbed D₂ transition of ⁸⁵Rb (transition frequency ω_0) by $\delta_{\text{MOT}} = \omega_L - \omega_0 = -2\pi \times 16.3$ MHz. The MOT cloud contains several million ⁸⁵Rb atoms and is used as a reservoir of cold atoms for loading the optical dipole trap. To load a single atom, the MOT cloud is positioned at the focus region of an aspheric lens with NA of 0.55 (AS-AHL12-10, Asphericon), located inside the vacuum and with a focal length of $f = 10$ mm and a working distance of $w_d = 7.6$ mm. The optical dipole trap is generated by focusing the incident trap laser beam (wavelength, $\lambda_{\text{trap}} = 784.65$ nm) to a waist radius of $w_0 = 1.8 \pm 0.2$ μm inside the MOT cloud. For a laser power of $P_{\text{trap}} = 2.5$ mW, we obtain an optical trapping potential with a depth of $U_{\text{trap}}/k_B = 1.66$ mK, corresponding to trap frequencies of $\omega_r = 2\pi \times 96$ kHz and $\omega_z = 2\pi \times 17$ kHz in the radial and axial directions, respectively. The photon scattering rate of the trapping light field amounts to 0.86 kHz.

The presence of an atom in the trap is registered by an increase in the photon detection rate from 120 s⁻¹ to 1,050 s⁻¹ for the case without spectral filtering (Extended Data Fig. 1). Here, we collect the fluorescence light with the same lens that we use for focusing the trap beam. Due to the microscopic trap volume, our trap operates in the collisional blockade regime⁴⁰ such that, at most, a single atom is present inside the trapping volume at any time (Extended Data Fig. 1). The collected fluorescence light is separated from the trapping light with a bandpass dichroic mirror centred at 780 nm that features a

linewidth of 3 nm (LL01-785-25, Semrock). We then couple the light into a single-mode fibre, which also acts as a spatial filter. The fibre-guided fluorescence is sent via the fibre-ring resonator filter to a fibre-based Hanbury Brown and Twiss set-up consisting of two fibre-coupled single-photon counting modules behind a 50/50 fibre-optic coupler. The two single-photon counting modules are connected to a field-programmable gate array-based time-tagger that records the arrival times of each detected photon.

Spectral filtering. Our fibre-based optical notch filter consists of a variable ratio coupler (F-CPL-830-N-FA, Newport) that allows setting of the coupling rate, κ_{ext} , into the resonator. A polarization controller is included in the fibre-ring section, such that the two polarization eigenmodes of the resonator are degenerate and the resonator acts as a polarization-independent filter. This is important for consistent spectral suppression of the collected atomic fluorescence. A section of the fibre ring is glued to a piezo-electric stack, which allows us to strain-tune the resonance frequency, ω_{res} . The resonator is passively stabilized by placing its whole set-up inside a thermally and acoustically insulating box, isolating the set-up from external environmental fluctuations. To compensate for residual, slow drifts of the resonance frequency, every 5 s we launch a stabilization light field at frequency ω_l into the resonator set-up, scan the resonator length, and set it such that the point of minimum transmission is reached. The resonator has a geometrical length of $l = 2.25 \pm 0.05$ m, yielding a free spectral range of $\nu_{\text{FSR}} = 89.0 \pm 0.5$ MHz. Extended Data Fig. 2 shows the on-resonance transmission of the resonator for different coupling rates κ_{ext} . From a fit to the data, we obtain an intrinsic resonator loss rate of $\kappa_0 = 2\pi \times 1.08 \pm 0.02$ MHz, which results in an unloaded resonator finesse of $\mathcal{F} = \pi\nu_{\text{FSR}}/\kappa_0 = 41.2 \pm 0.8$.

Analysis of measured correlation functions. To fit the theory to the measured correlation functions in Fig. 3, we perform the following procedure.

First, the measured correlation functions exhibit a weak bunching effect on a microsecond timescale, which originates from the diffusive motion of the trapped atoms through the complex intensity and polarization pattern of the MOT laser field⁴¹ (Extended Data Fig. 3). To account for this, we fit the function $1 + Ae^{|\tau|/\tau_b}$ to the data for large time delays $|\tau| \gg 1/2\gamma$, from which we obtain typical values of its amplitude $A = 1.38$ and decay time $\tau_b = 3.48 \mu\text{s}$ for the measurement without filtering ($\kappa_{\text{ext}} = 0$). For each $g^{(2)}$ measurement, our model is then adjusted such that the value $1 + A$ serves as the new baseline. Second, the finite temperature of the atom in the dipole trap gives rise to a temperature-dependent distribution of atomic positions in the trap and, consequently, of the a.c. Stark shifts. To account for this, we assume a thermal position distribution and fit the second-order correlation function of the unfiltered case ($\kappa_{\text{ext}} = 0$) with the atom temperature and the maximum a.c. Stark shift as free fit parameters. The latter takes into account that the atom experiences a substantial tensor light shift, which results in a Zeeman state-dependent transition frequency. From the fit, we obtain a temperature of $144 \pm 47 \mu\text{K}$ and a mean detuning of the atom from the MOT lasers of $\Delta/2\pi = -57.9 \pm 3.7$ MHz. These values are used to fit the data obtained for all other settings of the filter resonator.

Finally, for the measurements that incorporate the filter resonator, an additional experimental uncertainty occurs due to drifts of the narrow resonator absorption line with respect to the MOT laser frequency. To account for these residual resonator drifts in our model, we assume that the filter exhibits a Gaussian probability distribution of resonance frequencies with a width of σ centred around an average resonator-laser detuning $\delta = \omega_{\text{res}} - \omega_l$. Using this model, we fit all measured correlation functions in Fig. 3 with $\kappa_{\text{ext}} \neq 0$. From the results we obtain an average laser-resonator detuning of $\delta = -0.26 \pm 0.58$ MHz with a width of $\sigma = 1.92 \pm 0.36$ MHz.

Detection efficiency. From the atomic temperature obtained from the previous section, we calculate the distribution of saturation parameters S from which we obtain the expected scattering rates of the incoherent and coherent components. Together with the laser-filter detuning, we can then calculate the expected photon detection rate. We fit this model with the total photon detection efficiency, η , as the only free parameter to the data shown in the inset of Fig. 4. The fit yields $\eta = 0.136 \pm 0.002\%$, which agrees with the value expected from our collection efficiency of $\sim 1.3\%$, together with the propagation losses through the filter set-up and the limited detector efficiency of ~ 0.55 .

Correlation function at zero time delay versus filter setting. To evaluate the theory prediction of the zero-time-delay value of the second-order correlation as a function of κ_{ext} shown in Fig. 4, we use the approximate expression for $g^{(2)}(\tau)$ given in equation (19). Here, we use the temperature-induced distribution of S , the residual laser-resonator detunings and the photon detection efficiency η , which we obtained from previous measurements, as well as the mean detector background rates as parameters.

Photon-pair rate. To determine the number of detected photon pairs, we start with the histogram of measured coincidences and subtract the base level found for $|\tau| \gg 1/2\gamma$, which stems from accidental coincidences. By summing up all remaining coincidences within a time interval of ± 100 ns around $\tau = 0$ and dividing by the effective measurement time, we obtain the rate of detected photon pairs. Given our photon-pair detection efficiency $\eta^2/2$, we then determine the total rate of photon pairs scattered by the atom, $2n_{\text{meas}}^{(2)}/\eta^2$. For the case of strong suppression of the coherent component, that is, $t_F \approx 0$, these detected pairs all originate from the incoherently scattered light, so the rate of scattered photon pairs should be given by $n_{\text{inc}}/2$ (equation (6)).

Data availability

Source data for all figures in this study are available in an open-access repository⁴².

Code availability

The code used for data analysis during this study is available, upon reasonable request, from the corresponding authors.

References

- Schneeweiss, P., Zeiger, S., Hoinkes, T., Rauschenbeutel, A. & Volz, J. Fiber ring resonator with a nanofiber section for chiral cavity quantum electrodynamics and multimode strong coupling. *Opt. Lett.* **42**, 85–88 (2017).
- Neelen, R. C., Boersma, D. M., van Exter, M. P., Nienhuis, G. & Woerdman, J. P. Spectral filtering within the Schawlow-Townes linewidth of a semiconductor laser. *Phys. Rev. Lett.* **69**, 593–596 (1992).
- Kusmieriek, K. J. et al. Higher-order mean-field theory of chiral waveguide QED. *SciPost Phys. Core* **6**, 041 (2023).
- Moqanaki, A., Massa, F. & Walther, P. Novel single-mode narrow-band photon source of high brightness tuned to cesium D₂ line. *APL Photonics* **4**, 090804 (2019).
- Schlosser, N., Reymond, G., Protzenko, I. & Grangier, P. Sub-Poissonian loading of single atoms in a microscopic dipole trap. *Nature* **411**, 1024–1027 (2001).
- Gomer, V. et al. Decoding the dynamics of a single trapped atom from photon correlations. *Appl. Phys. B* **67**, 689–697 (1998).
- Masters, L. et al. *On the Simultaneous Scattering of Two photons by a Single Two-Level Atom* (HU Berlin edoc-Server, 2023); <https://doi.org/10.18452/26730>

Acknowledgements

We acknowledge funding by the Alexander von Humboldt Foundation in the framework of the Alexander von Humboldt Professorship endowed by the Federal Ministry of Education and Research, as well as the European Commission under project DAALI (no. 899275). X.-X.H. acknowledges a Humboldt Research Fellowship by the Alexander von Humboldt Foundation. M.C. and M.S. acknowledge support by the European Commission (Marie Skłodowska-Curie IF grants nos. 101029304 and 896957).

Author contributions

L.M., J.V. and A.R. designed the set-up and conceived the experiment. L.M., X.-X.H., G.M. and L.P. performed the experimental work. J.V., M.C. and M.S. developed the theoretical model. L.M. and X.-X.H. analysed the data. All authors contributed to the discussion of the results and manuscript preparation.

Competing interests

The authors declare no competing interests.

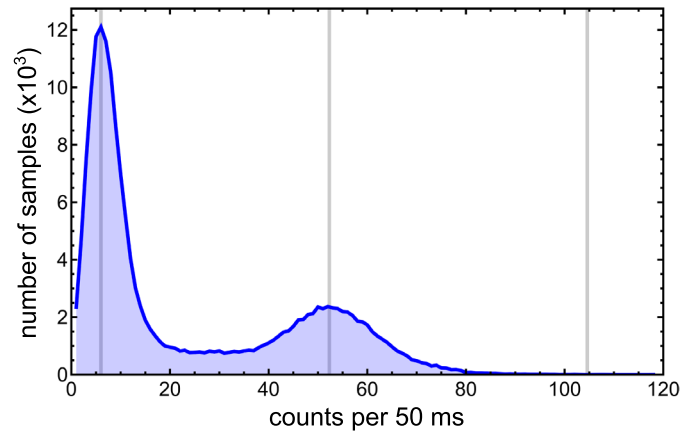
Additional information

Extended data is available for this paper at <https://doi.org/10.1038/s41566-023-01260-7>.

Correspondence and requests for materials should be addressed to Arno Rauschenbeutel or Jürgen Volz.

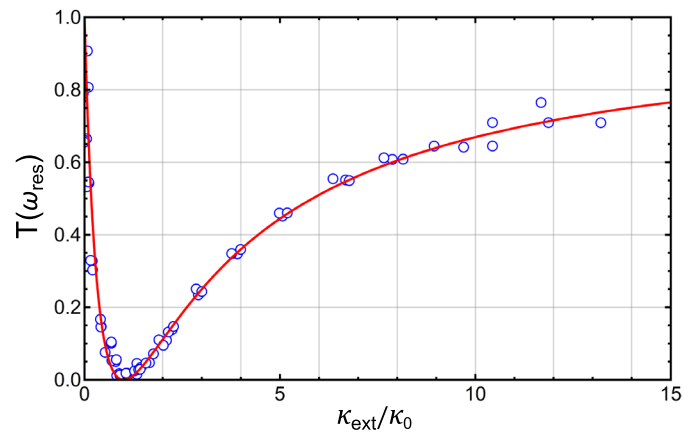
Peer review information *Nature Photonics* thanks Fabrice Laussy and the other, anonymous, reviewers for their contribution to the peer review of this work.

Reprints and permissions information is available at www.nature.com/reprints.

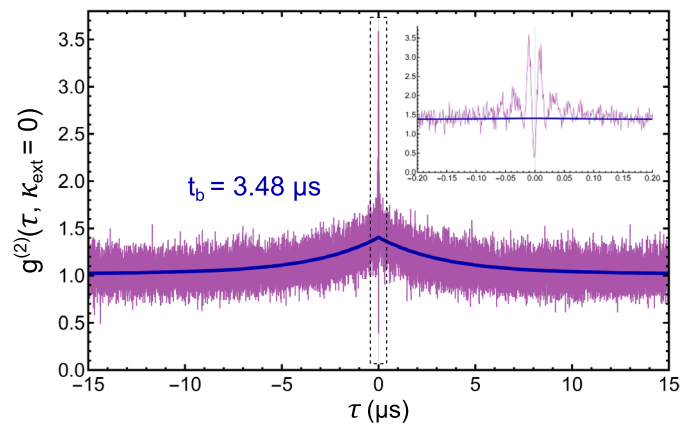


Extended Data Fig. 1 | Histogram of the detected photon count rate originating from the trap volume. Without spectral filtering, we observe an increase in the most likely count rate from a background of 120 s^{-1} , to 1050 s^{-1}

when one atom is trapped. The absence of higher count rates indicates the sub-poissonian occupation statistics due to the collisional blockade effect present in microscopic optical traps⁴⁰.



Extended Data Fig. 2 | Characterisation of the spectral filter. Measured on-resonance power transmission $|t_F(\omega_{\text{res}})|^2$ as a function of κ_{ext} (blue data points). The solid red line is a fit according to Eq. (13), yielding an intrinsic resonator loss rate of $\kappa_0/2\pi = 1.08 \pm 0.02$ MHz.



Extended Data Fig. 3 | Long-term behaviour of the second order correlation function. A weak bunching effect arising from diffusive atomic motion is apparent. It exhibits a decay time of $t_b = 3.48 \mu\text{s}$ for the dataset with $\kappa_{\text{ext}} = 0$, see main text. Inset: zoom on the area indicated by the dashed line.